INTERNATIONAL JOURNAL FOR NUMERICAL METHODS IN FLUIDS
Int. J. Numer. Meth. Fluids 2010; **63**:517–532
Published online 3 June 2009 in Wiley InterScience (www.interscience.wiley.com). DOI: 10.1002/fld.2082

SHORT COMMUNICATION

Free convection of a dusty-gas flow along a semi-infinite vertical cylinder

G. Palani*,† and Kwang-Yong Kim

Department of Mechanical Engineering, Inha University, Incheon 402-751, Republic of Korea

SUMMARY

An analysis is performed to study the free convection of a dusty-gas flow along a semi-infinite isothermal vertical cylinder. The governing equations of the flow problem are transformed into non-dimensional form and the resulting nonlinear, coupled parabolic partial differential equations have been solved numerically using an implicit finite difference scheme of Crank–Nicholson type. The flow variables such as gas–velocity, dust-particle velocity and temperature, shearing stress and heat transfer coefficients are calculated numerically for various parameters occurring in the problem. It is observed that due to the presence of dust particles, the gas velocity is found to decrease. Copyright © 2009 John Wiley & Sons, Ltd.

Received 12 October 2008; Revised 29 March 2009; Accepted 9 April 2009

KEY WORDS: cylinder; dust particle; finite difference; transient flow; Grashof number; mass concentration

1. INTRODUCTION

Transient natural convection flows over vertical bodies have a wide range of applications in engineering and technology. These kinds of problems are frequently encountered in the study of enhanced heat transfer around various kinds of electrical and electronics devices and nuclear reactors. In manufacturing processes such as hot extrusion, metal forming and crystal growing, heat transfer effects play an important role. In particular, the study of enhanced heat transfer is very useful in cylindrical surfaces. Sparrow and Gregg [1] presented the approximate solution for the laminar buoyant flow of air bathing a vertical cylinder heated with a prescribed surface temperature using similarity method. Minkowycz and Sparrow [2] obtained the solution for the same problem using the nonsimilarity method. Lee *et al.* [3] attempted the natural convection along a slender vertical cylinder with variable surface temperature. The governing equations are

*Correspondence to: G. Palani, Department of Mechanical Engineering, Inha University, Incheon 402-751, Republic of Korea.
†E-mail: gpalani32@yahoo.co.in

Contract/grant sponsor: BK21 Research Programme

steady and the solutions are obtained using spline interpolation. Ganesan and Rani [4] studied the transient natural convection flow over a vertical cylinder with variable surface temperatures. The governing equations are solved using an implicit finite difference method.

In all the above papers, the fluid considered was viscous, incompressible and free from impurities. However, in nature, the fluid in pure form is rarely available. Air and water contain impurities like dust particles and foreign bodies.

A dusty fluid is a mixture of fluid and fine dust particles. Its study is important in areas like environmental pollution, smoke emission from vehicles, emission of effluents from industries, cooling effects of air conditioners, flying ash produced from thermal reactors, and formation of raindrops, etc. In addition, it is useful in the study of lunar ash flow, which explains many features of the lunar soil. Other important applications of dust particles in boundary layers include soil erosion by natural winds and dust entrainment in a cloud during nuclear explosion. In addition, such flows occur in a wide range of areas of technical importance such as fluidization, flow in rocket tubes, combustion, paint spraying and more recently, blood flows in capillaries. Saffman [5] discussed the stability of the laminar flow of a dusty gas in which the dust particles are uniformly distributed. Liu [6] studied the flow induced by an oscillating infinite flat plate in a dusty gas. Michael and Miller [7] investigated the motion of dusty gas with a uniform distribution of the dust particles occupied in the semi-infinite space above a rigid plane boundary. Micheal [8] considered the effect on the steady flow past a sphere of a uniform upstream distribution of dust particles having a small relaxation time. Soundalgekar and Gokhale [9] studied the flow of a dusty gas past an impulsively started, infinite vertical plate by employing an implicit finite difference scheme. Flow of a dusty gas past a uniformly accelerated horizontal plate was presented by Das *et al.* [10]. Palani and Ganesan [11] studied the heat transfer effects on dusty-gas flow past a semi-infinite inclined plate using a finite difference technique.

The unsteady natural convection flow of a dusty gas past a semi-infinite isothermal vertical cylinder has received less attention in the literature. Hence, in the present investigation, our attention is focused on the flow of dusty gas along a semi-infinite isothermal vertical cylinder.

2. MATHEMATICAL ANALYSIS

A problem of transient, laminar, two-dimensional flow of a dusty gas along a semi-infinite isothermal vertical cylinder is considered here. The analysis of the present paper is based on the following assumption:

1. Consider a vertical cylinder of radius r_0, which is aligned in a quiescent ambient fluid at temperature T'_∞ .
2. The x-coordinate is measured upward in the axial direction from the leading edge of the cylinder and r-coordinate is measured in the radial direction from the axis of the cylinder as shown in Figure 1.
3. The gravitational acceleration g is acting downward.
4. Initially at time $t' \leqslant 0$, it is assumed that the cylinder and the fluid are at the same ambient temperature T'_∞. When at time $t' \geqslant 0$, the temperature of the cylinder is maintained to be $T'_w (> T'_\infty)$.
5. All the fluid properties are assumed to be constant except the influence of the density variation that induces the buoyancy force.

DOI: 10.1002/fld

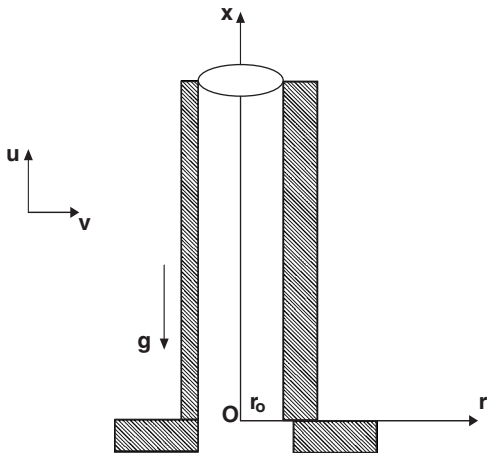

Figure 1. Physical system of the problem.

6. The effect of viscous dissipation is not considered in the energy equation.
7. There is no chemical reaction between the diffusing species and the fluid.
8. It is assumed that the dust particles are uniform in size and shape and they are uniformly distributed.
9. The number density of the dust particles is constant throughout the motion.
10. Interaction between the particles themselves has not been considered.

By employing laminar boundary layer flow assumptions due to Saffman [5] and the Boussinesq approximation, the governing conservation equations [2–4] can be written as

Equation for dusty gas:

$$\frac{\partial(ru)}{\partial x}+\frac{\partial(rv)}{\partial r}=0 \tag{1}$$

$$\frac{\partial u}{\partial t'}+u\frac{\partial u}{\partial x}+v\frac{\partial u}{\partial r}=g\beta(T'-T'_\infty)+\frac{v}{r}\frac{\partial}{\partial r}\left(r\frac{\partial u}{\partial r}\right)+\frac{\kappa_1 N_0}{\rho}(u_p-u) \tag{2}$$

The forces exerted on the dust by the gas are equal and opposite to the force exerted on the gas by dust, so that the equation of the motion of dust [5, 9, 10] is

Equation for dust particles:

$$\frac{\partial N_0}{\partial t'}+\frac{\partial(N_0 r u_p)}{\partial x}+\frac{\partial(N_0 r v_p)}{\partial r}=0 \tag{3}$$

$$m\left[\frac{\partial u_p}{\partial t'}+u_p\frac{\partial u_p}{\partial x}+v_p\frac{\partial u_p}{\partial r}\right]=-mg+\kappa_1(u-u_p) \tag{4}$$

DOI: 10.1002/fld

Equation for energy:

$$\rho C_p\left[1+\frac{mN_0}{\rho}\frac{C_{p2}}{C_p}\right]\left[\frac{\partial T'}{\partial t'}+u\frac{\partial T'}{\partial x}+v\frac{\partial T'}{\partial r}\right]=\frac{k}{r}\frac{\partial}{\partial r}\left(r\frac{\partial T'}{\partial r}\right) \tag{5}$$

By our assumption, the number N_0 density of dust particles is assumed to be constant throughout the motion. Hence, Equation (3) reduces to

$$\frac{\partial(ru_p)}{\partial x}+\frac{\partial(rv_p)}{\partial r}=0 \tag{6}$$

If the dust particles are spheres of radius d, then Stokes resistance coefficient is $\kappa_1=6\pi\mu d$, with μ being the viscosity of the fluid.
The initial and boundary conditions are

$$\begin{aligned}
&t'\leqslant 0\colon\ u=0,\quad u_p=0,\quad v=0,\quad v_p=0,\quad T'=T'_\infty \quad \text{for all } x\geqslant 0 \text{ and } r\geqslant 0\\
&t'>0\colon\ u=0,\quad u_p=0,\quad v=0,\quad v_p=0,\quad T'=T'_w \quad \text{at } r=r_0\\
&\qquad\ u=0,\quad u_p=0,\quad T'=T'_\infty \quad \text{at } x=0\\
&\qquad\ u\to 0,\quad u_p\to 0,\quad T'\to T'_\infty \quad \text{as } r\to\infty
\end{aligned} \tag{7}$$

As a prelude to solution, the governing equations (1), (2), (4)–(6) are first transformed into a dimensionless form. To do this, one introduces the following non-dimensional quantities as:

$$\begin{aligned}
&X=\frac{x}{r_0}Gr^{-1},\quad R=\frac{r}{r_0},\quad U=\frac{ur_0}{v}Gr^{-1},\quad U_p=\frac{u_pr_0}{v}Gr^{-1}\\
&V=\frac{vr_0}{v},\quad V_p=\frac{v_pr_0}{v},\quad t=\frac{vt'}{r_0^2},\quad T=\frac{T'-T'_\infty}{T'_w-T'_\infty}\\
&Gr=\frac{g\beta r_0^3(T'_w-T'_\infty)}{v^2},\quad Pr=\frac{\rho vC_p}{k},\quad h=\frac{fC_{p2}}{C_p},\quad f=\frac{mN_0}{\rho}\\
&\kappa=\frac{\kappa_1r_0^2}{mv},\quad g_1=\frac{gr_0^3}{v^2}Gr,\quad \lambda=Pr(1+h)
\end{aligned} \tag{8}$$

Equations (1), (2), (4)–(6) are reduced to the following non-dimensional form:

$$\frac{\partial U}{\partial X}+\frac{\partial V}{\partial R}+\frac{V}{R}=0 \tag{9}$$

$$\frac{\partial U}{\partial t}+U\frac{\partial U}{\partial X}+V\frac{\partial U}{\partial R}=T+\frac{\partial^2U}{\partial R^2}+\frac{1}{R}\frac{\partial U}{\partial R}+f\kappa(U_p-U) \tag{10}$$

$$\frac{\partial U_p}{\partial X}+\frac{\partial V_p}{\partial R}+\frac{V_p}{R}=0 \tag{11}$$

DOI: 10.1002/fld

$$\frac{\partial U_p}{\partial t}+U_p\frac{\partial U_p}{\partial X}+V_p\frac{\partial U_p}{\partial R}=-g_1 Gr^{-2}+\kappa(U-U_p) \tag{12}$$

$$\frac{\partial T}{\partial t}+U\frac{\partial T}{\partial X}+V\frac{\partial T}{\partial R}=\frac{1}{\lambda}\left[\frac{\partial^2 T}{\partial R^2}+\frac{1}{R}\frac{\partial T}{\partial R}\right] \tag{13}$$

The corresponding initial and boundary conditions in dimensionless form are as follows:

$$\begin{aligned}
&t\leqslant 0\colon\ U=0,\quad U_p=0,\quad V=0,\quad V_p=0,\quad T=0\quad \text{for all } X\geqslant 0 \text{ and } R\geqslant 0\\
&t>0\colon\ U=0,\quad U_p=0,\quad V=0,\quad V_p=0,\quad T=1\quad \text{at } R=1\\
&\qquad U=0,\quad U_p=0,\quad T=0\quad \text{at } X=0\\
&\qquad U\to 0,\quad U_p\to 0,\quad T\to 0\quad \text{as } R\to\infty
\end{aligned} \tag{14}$$

Non-dimensional forms of the local and average skin friction and Nusselt number are:

$$\tau_X=Gr\left(\frac{\partial U}{\partial R}\right)_{R=1} \tag{15}$$

$$\bar{\tau}=Gr\int_0^1\left(\frac{\partial U}{\partial R}\right)_{R=1}\mathrm{d}X \tag{16}$$

$$Nu_X=-XGr\left(\frac{\partial T}{\partial R}\right)_{R=1}\Big/T_{R=1} \tag{17}$$

$$\bar{N}u=-Gr\int_0^1\left[\left(\frac{\partial T}{\partial R}\right)_{R=1}\Big/T_{R=1}\right]\mathrm{d}X \tag{18}$$

3. NUMERICAL TECHNIQUES

The two-dimensional, nonlinear, unsteady and coupled partial differential equations (9)–(13) under the initial and boundary conditions (14) are solved using an implicit finite difference scheme of Crank–Nicolson type. The finite difference equations corresponding to Equations (9)–(13) are as follows:

$$\frac{\left[U_{i,j}^{n+1}-U_{i-1,j}^{n+1}+U_{i,j}^{n}-U_{i-1,j}^{n}+U_{i,j-1}^{n+1}-U_{i-1,j-1}^{n+1}+U_{i,j-1}^{n}-U_{i-1,j-1}^{n}\right]}{4\triangle X}$$

$$+\frac{\left[V_{i,j}^{n+1}-V_{i,j-1}^{n+1}+V_{i,j}^{n}-V_{i,j-1}^{n}\right]}{2\triangle R}+\frac{V_{i,j}^{n+1}}{1+(j-1)\triangle R}=0 \tag{19}$$

$$\frac{\left[U_{i,j}^{n+1}-U_{i,j}^{n}\right]}{\triangle t}+U_{i,j}^{n}\frac{\left[U_{i,j}^{n+1}-U_{i-1,j}^{n+1}+U_{i,j}^{n}-U_{i-1,j}^{n}\right]}{2\triangle X}+V_{i,j}^{n}\frac{\left[U_{i,j+1}^{n+1}-U_{i,j-1}^{n+1}+U_{i,j+1}^{n}-U_{i,j-1}^{n}\right]}{4\triangle R}$$

DOI: 10.1002/fld

$$=\frac{1}{2}\left[T_{i,j}^{n+1}+T_{i,j}^{n}\right]+\frac{\left[U_{i,j-1}^{n+1}-2U_{i,j}^{n+1}+U_{i,j+1}^{n+1}+U_{i,j-1}^{n}-2U_{i,j}^{n}+U_{i,j+1}^{n}\right]}{2(\triangle R)^2}$$

$$+\frac{\left[U_{i,j+1}^{n+1}-U_{i,j-1}^{n+1}+U_{i,j+1}^{n}-U_{i,j-1}^{n}\right]}{4[1+(j-1)\triangle R]\triangle R}+f\kappa\left[\left(\frac{U_{p\ i,j}^{n+1}+U_{p\ i,j}^{n}}{2}\right)-\left(\frac{U_{i,j}^{n+1}+U_{i,j}^{n}}{2}\right)\right] \tag{20}$$

$$\frac{\left[U_{p\ i,j}^{n+1}-U_{p\ i-1,j}^{n+1}+U_{p\ i,j}^{n}-U_{p\ i-1,j}^{n}+U_{p\ i,j-1}^{n+1}-U_{p\ i-1,j-1}^{n+1}+U_{p\ i,j-1}^{n}-U_{p\ i-1,j-1}^{n}\right]}{4\triangle X}$$

$$+\frac{\left[V_{p\ i,j}^{n+1}-V_{p\ i,j-1}^{n+1}+V_{p\ i,j}^{n}-V_{p\ i,j-1}^{n}\right]}{2\triangle R}+\frac{V_{p\ i,j}^{n+1}}{1+(j-1)\triangle R}=0 \tag{21}$$

$$\frac{\left[U_{p\ i,j}^{n+1}-U_{p\ i,j}^{n}\right]}{\triangle t}+U_{p\ i,j}^{n}\frac{\left[U_{p\ i,j}^{n+1}-U_{p\ i-1,j}^{n+1}+U_{p\ i,j}^{n}-U_{p\ i-1,j}^{n}\right]}{2\triangle X}$$

$$+V_{p\ i,j}^{n}\frac{\left[U_{p\ i,j+1}^{n+1}-U_{p\ i,j-1}^{n+1}+U_{p\ i,j+1}^{n}-U_{p\ i,j-1}^{n}\right]}{4\triangle R}$$

$$=-g_1 Gr^{-2}+\kappa\left[\left(\frac{U_{i,j}^{n+1}+U_{i,j}^{n}}{2}\right)-\left(\frac{U_{p\ i,j}^{n+1}+U_{p\ i,j}^{n}}{2}\right)\right] \tag{22}$$

$$\frac{\left[T_{i,j}^{n+1}-T_{i,j}^{n}\right]}{\triangle t}+U_{i,j}^{n}\frac{\left[T_{i,j}^{n+1}-T_{i-1,j}^{n+1}+T_{i,j}^{n}-T_{i-1,j}^{n}\right]}{2\triangle X}$$

$$+\ V_{i,j}^{n}\frac{\left[T_{i,j+1}^{n+1}-T_{i,j-1}^{n+1}+T_{i,j+1}^{n}-T_{i,j-1}^{n}\right]}{4\triangle R}$$

$$=\frac{\left[T_{i,j-1}^{n+1}-2T_{i,j}^{n+1}+T_{i,j+1}^{n+1}+T_{i,j-1}^{n}-2T_{i,j}^{n}+T_{i,j+1}^{n}\right]}{2\lambda(\triangle R)^2}$$

$$+\frac{\left[T_{i,j+1}^{n+1}-T_{i,j-1}^{n+1}+T_{i,j+1}^{n}-T_{i,j-1}^{n}\right]}{4\lambda[1+(j-1)\triangle R]\triangle R} \tag{23}$$

The region of integration is considered as a rectangle with sides $X_{\min}(=0), X_{\max}(=1)$ and $R_{\min}(=1), R_{\max}(=21)$, where $R_{\max}$ corresponds to $R=\infty$, which lies very well outside the momentum and energy boundary layers. An 50×100 uniform grid for the fluid flow was selected.

DOI: 10.1002/fld

These grid sizes were chosen, after several grids, to ensure grid independence of the results while obtaining the fastest convergence. The maximum of R was chosen as 21 after some preliminary investigations so that the last two of the boundary conditions (14) are satisfied.

During any one time step, the coefficients $U^n_{p\,i,j}, U^n_{i,j}, V^n_{i,j}$ and $V^n_{p\,i,j}$ appearing in the difference equations are treated as constants. The values of T, U_p, U, V_p and V at time level $(n+1)$ using known values at previous time level (n) are calculated as follows. The finite difference equation (23) at every internal nodal point on a particular i-level constitutes a system of equations. Such a system of equations is solved by Thomas algorithm as described by Carnahan *et al.* [12]. Thus, the values of T are known at every internal nodal point on a particular i at $(n+1)$th time level. Similarly, the values of U_p and U are calculated from Equations (22) and (20), respectively. Then the values of V_p and V are calculated explicitly from Equations (21) and (19), respectively, at every internal nodal point at particular i-level at $(n+1)$th time level. This process is repeated for various i-levels. Thus, the values of T, U_p, U, V_p and V are known at all grid points in the rectangular region at $(n+1)$th time level. The iterative process is repeated for several time steps until steady state is reached. The steady-state solution is assumed to have been reached, when the absolute difference between the values of U_p, U and T at two consecutive time steps is less than 10^{-5} at each grid points. After experimenting with a few sets of mesh sizes, the mesh has been fixed at the level $\triangle X = 0.02, \triangle R = 0.2$ and the time step $\triangle t = 0.01$. For this case, the spatial mesh sizes were reduced by 50% in one direction, then in both directions, and the results compared. It is observed that when mesh size is reduced by 50% in the X-direction and the R-direction the results differ only in the fourth decimal place. Hence, the above mentioned sizes have been considered as an appropriate mesh sizes for calculation.

The truncation error in the finite difference scheme is $O(\triangle t^2 + \triangle R^2 + \triangle X)$ and it tends to zero as $\triangle t, \triangle R$ and $\triangle X \to 0$, which shows that the system is compatible. In addition, the Crank–Nicholson system is unconditionally stable for natural convection flow [4]. Thus, the compatible and stability ensure convergence.

The derivatives involved in Equations (15)–(18) are evaluated using a five-point approximation formula and then the integrals are evaluated using Newton–Cotes closed integration formula.

4. RESULTS AND DISCUSSION

To validate the current numerical procedure, the computed velocity profiles are compared with the results of Lee *et al.* [3] in Figure 2 for the steady, isothermal case without dust particles and with $Pr = 0.7$. There are no better experimental or analytical studies to be compared with the present problem.

During the initial period, the body forces have not had sufficient time to generate any appreciable motion in the fluid. Hence, both velocity components are negligible for small time 't'. During this initial transient regime, the heat transfer process is dominated by pure heat conduction. The temperature distribution at early times is therefore the same as the transient conduction problem in a semi-infinite solid. The temperature distribution in a semi-infinite solid is given by the following equation [13, 14]:

$$T' = \left(\frac{r_0}{r}\right)^{1/2} \operatorname{erfc}\left(\frac{r - r_0}{2\sqrt{\alpha t'}}\right) \tag{24}$$

DOI: 10.1002/fld

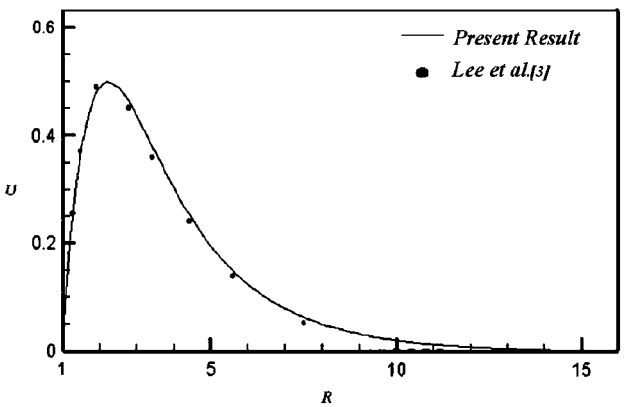

Figure 2. Comparison of velocity profiles.

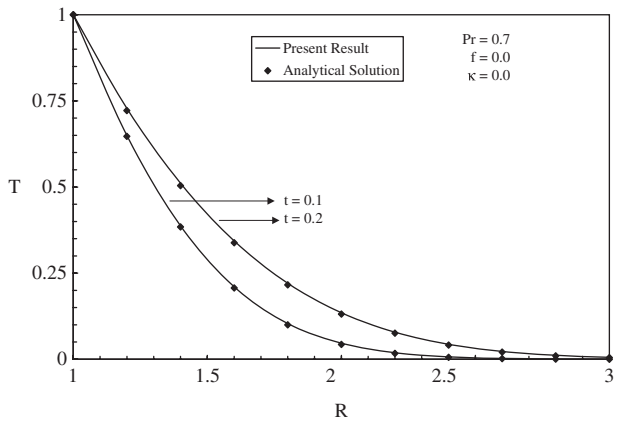

Figure 3. Comparison of temperature profiles for the conduction of semi-infinite solids.

with the initial and boundary conditions:

$$t' \leqslant 0\colon\ T' = T'_{\infty} \quad \text{for all } r$$
$$t' > 0\colon\ T' = T'_{w} \quad \text{at } r = r_0$$

By Introducing the non-dimensional quantities defined in Equation (8), the transient temperature distribution in a semi-infinite solid can be written as

$$T = R^{-1/2}\,\mathrm{erfc}\left(\frac{R-1}{2\sqrt{t/Pr}}\right) \tag{25}$$

with the initial and boundary conditions:

$$t \leqslant 0\colon\ T = 0 \quad \text{for all } R$$
$$t > 0\colon\ T = 1 \quad \text{at } R = 1$$

DOI: 10.1002/fld

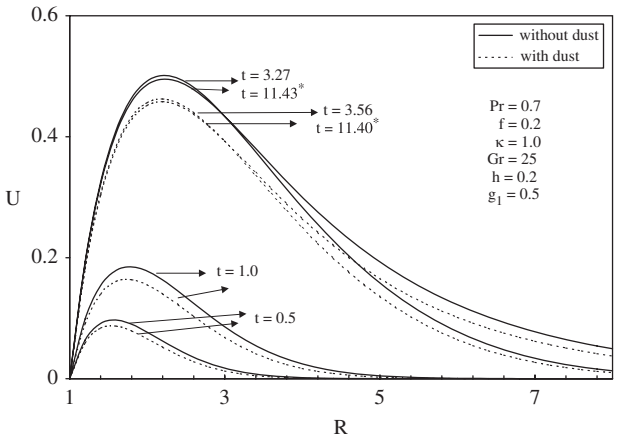

Figure 4. Transient velocity profiles at $X = 1.0$ (*-steady state).

Figure 3 shows that the comparison between the transient temperature distribution calculated by Equation(20) and by the current finite difference method at two different early times. They are found to be in an excellent agreement and this shows that the current finite difference methods are valid for this type of transient problem.

The velocity profiles for a gas with and without dust particles are shown in Figure 4. The velocity of the gas increases with time until a temporal maximum is reached and thereafter a moderate reduction is observed until the steady state is reached. However, due to the presence of dust particles, the maximum velocity of the gas decreases since these dust particles oppose the motion of the gas. When t is small, the effects of dust particles are not significant and when t is very large, the dust particles have a more significant influences on the velocity of gas. The difference between the temporal maximum and steady-state gas velocity is reduced due to the presence of dust particles. Also it is observed that the steady state is reached earlier when dust particles are presented in the gas. In Figure 5, the temperature profiles of the fluid are plotted with and without the dust particles. The temperature of the fluid without dust particles is higher in comparison with the case where dust particles are present, since these dust particles carry away heat and the fluid is cooled.

The effects of varying the dust parameters f (mass concentration), κ (dust parameter) and h (dust parameter) on dusty-gas velocity are studied in detail and are shown graphically in Figures 6 and 7. It is observed that the velocity is maximum near the upstream and decreases in the flow direction. An increase in the mass concentration of the dust leads to a fall in the gas velocity, since these dust particles oppose the motion of the gas. Time taken to reach the steady state increases due to increase in the value of f (the mass concentration of the dust). Also it is observed that the difference between the temporal maximum and steady state decreases due to increase in the mass concentration of dust. The velocity of the gas decreases as κ (dust parameter) increases. Owing to increase in the value of h, the velocity of the gas is found to decrease. More time is required to reach the steady state for lower values of h.

The influence of the dust parameters f, κ and h on dust-particle velocity is shown in Figures 8 and 9. According to our numerical results, the velocity of the dust particles increases with an

DOI: 10.1002/fld

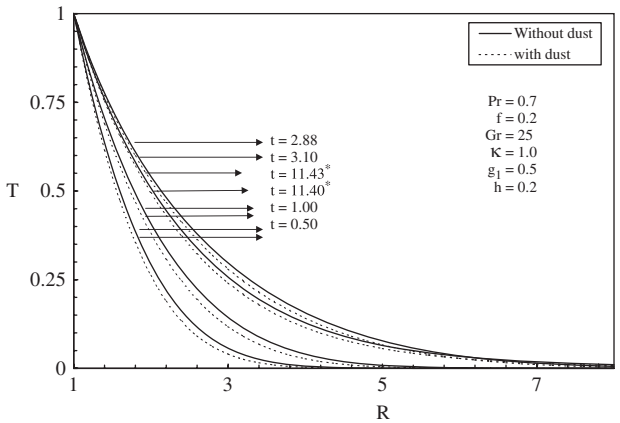

Figure 5. Transient temperature profiles at $X = 1.0$ (*-steady state).

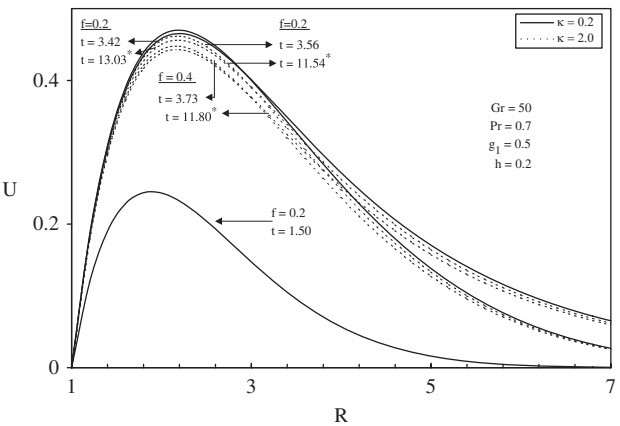

Figure 6. Transient dusty-gas velocity profiles at $X = 1.0$ for different f and κ (*-steady state).

increasing value of dust parameter κ. An increase in the mass concentration of the dust particle and the velocity of dust particles are found to decrease; this is quite expected. Also, it is observed that the velocity of the dust particles decreases by the increasing value of h.

Figures 10 and 11 show that the transient temperature profiles at their temporal maximum, earlier times and steady state against the axial coordinate R at $X = 1.0$ for different values of dust parameters f, κ and h. When t is small, the effect of f on temperature field is nil, but the temperature of the fluid containing dust particles increases as the mass concentration of the dust particle increases at the temporal maximum and steady state. It is observed that the temperature increases as κ increases. The time taken to reach the steady state decreases as κ increases. Also, it is noticed that temperature of the fluid decreases as h increases. Steady-state temperature profiles are attained at an early stage for higher values of h.

DOI: 10.1002/fld

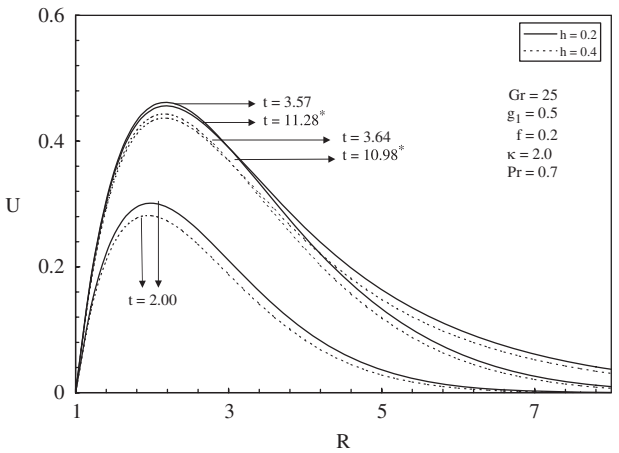

Figure 7. Transient dusty-gas velocity profiles at $X = 1.0$ for different h (*-steady state).

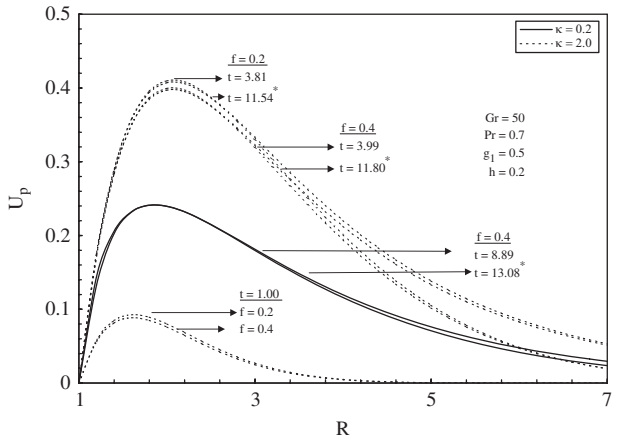

Figure 8. Transient dust-particle velocity profiles at $X = 1.0$ for different f and κ (*-steady state).

The steady-state local skin friction for various values of dust parameters f, κ and h is presented in Figure 12. Where the skin friction increases as X increases. An increase in the mass concentration of dust causes a fall in the local wall shear stress. It is observed that the local skin friction decreases as κ and h increase.

Local Nusselt number for different values of f, κ and h is shown in Figure 13. The rate of heat transfer decreases with increasing mass concentration of the dust. Also from the figure, we see that the Nusselt number decreases as κ increases, but it increases as h increases.

The average values of skin friction and Nusselt number are plotted in Figures 14 and 15, respectively. Average skin friction increases with time throughout the transient period and steady-state level. Figure 14 shows that an increase in the mass concentration of dust, the average skin

DOI: 10.1002/fld

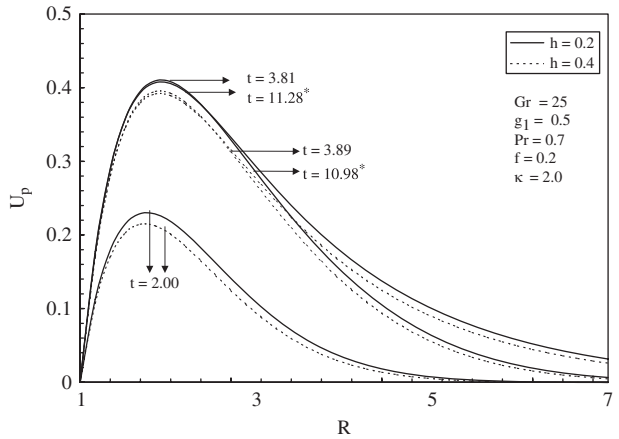

Figure 9. Transient dust particle velocity profile at $X = 1.0$ for different h (*-steady state).

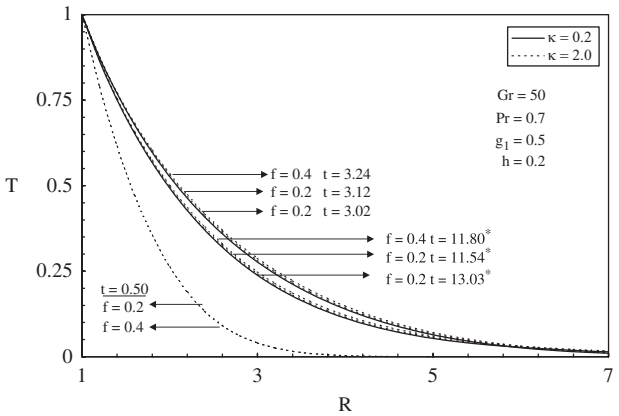

Figure 10. Transient temperature profiles at $X = 1.0$ for different f and κ (*-steady state).

friction is found to decrease. Also, it shows that average skin friction increases as κ and h decreases. From Figure 15, we observe that an increase in the mass concentration of the dust, the average Nusselt number is found to increase. It is observed that average Nusselt number decreases as h increases and also that it decreases as κ increases.

5. CONCLUSION

A numerical study has been performed for the flow of a fluid along a semi-infinite isothermal vertical cylinder, taking into account the effect of dust particles. A family of governing partial

DOI: 10.1002/fld

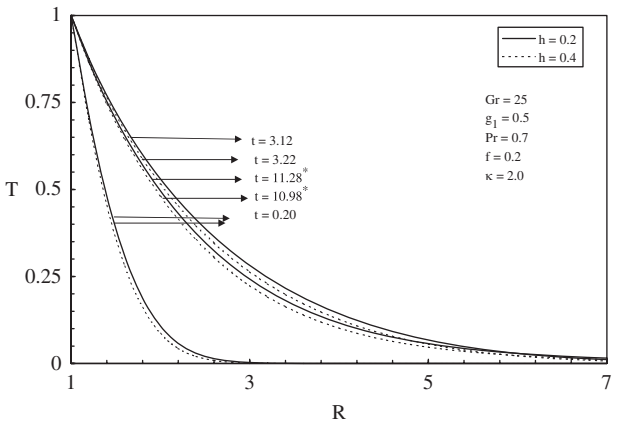

Figure 11. Transient temperature profiles at $X = 1.0$ for different h (*-steady state).

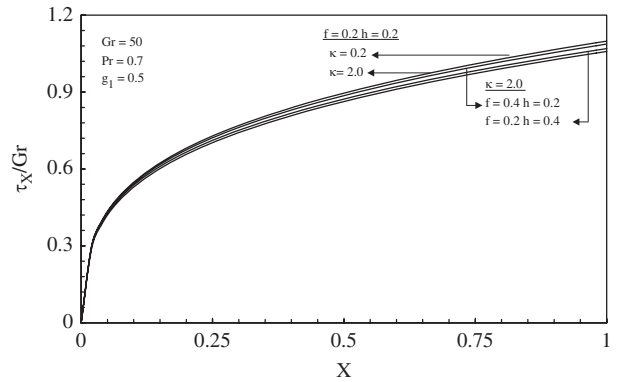

Figure 12. Local skin friction.

differential equations is solved by an implicit finite difference scheme of Crank–Nicholson type. The effect of various dust parameters f, κ and h on dusty-gas velocity, dust-particle velocity, shearing stress and local heat transfer is studied in detail. Conclusions of the study are as follows:

1. The difference between the temporal maximum and steady state of gas velocity is reduced due to the presence of dust particles.
2. An increase in the mass concentration of the dust leads to a fall in the gas velocity.
3. The velocity of the dust particles increases with an increasing value of dust parameter κ.
4. Steady-state temperature profiles attain at an early stage for the higher values of h.
5. An increase in the mass concentration of dust, the average skin friction is found to decrease.
6. It is observed that average Nusselt number decreases as h increases.

DOI: 10.1002/fld

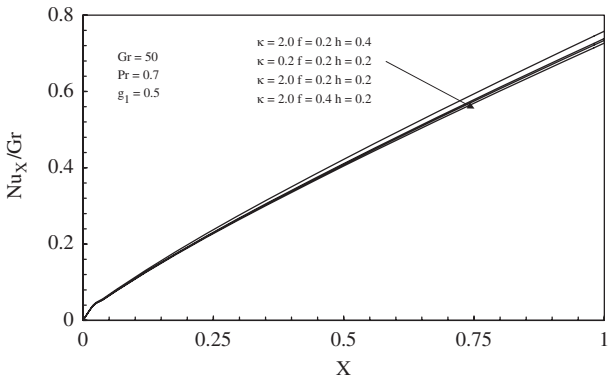

Figure 13. Local Nusselt number.

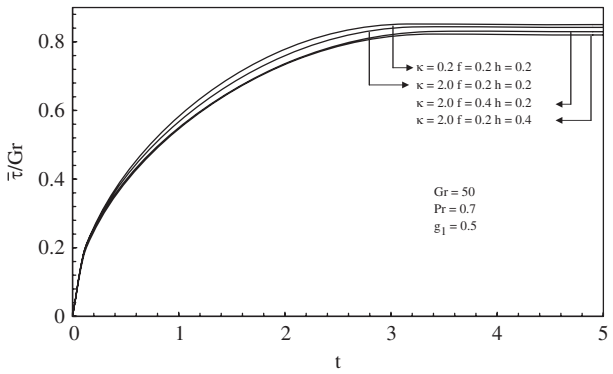

Figure 14. Average skin friction.

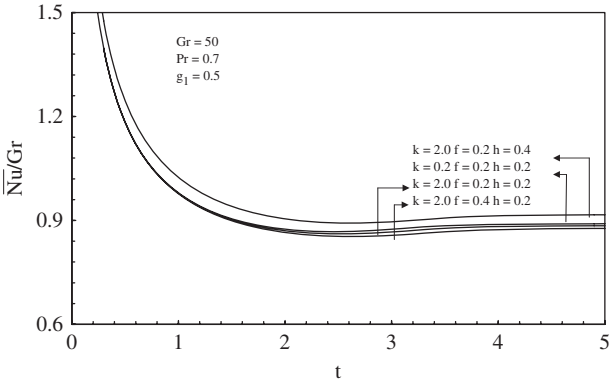

Figure 15. Average Nusselt number.

DOI: 10.1002/fld

NOMENCLATURE

C_p	specific heat of fluid at constant pressure
C_{p2}	specific heat of the particle at constant pressure
d	radius of dust particle
f	mass concentration of dust
g	acceleration due to gravity
g_1	non-dimensional dust parameter
Gr	Grashof number
h	non-dimensional dust parameter
k	thermal conductivity
m	mass of a dust particle
N_0	number density of small particle
Nu_X	dimensionless local Nusselt number
$\overline{Nu}$	dimensionless average Nusselt number
Pr	Prandtl number
r	radial coordinate
r_0	radius of cylinder
R	dimensionless radial coordinate
T'	temperature
T	dimensionless temperature
t'	time
t	dimensionless time
u, v	velocity components of dusty gas in the x, r-directions, respectively
u_p, v_p	velocity components of dust particles in the x, r-directions, respectively
U, V	dimensionless velocity components of dusty gas in the X, R-directions, respectively
U_p, V_p	dimensionless velocity components of dust particles in the X, R-directions, respectively
x	axial coordinate measured vertically
X	dimensionless axial coordinate

Greek symbols

κ_1	Stokes resistance coefficient
κ	non-dimensional parameter
β	volumetric coefficient of thermal expansion
ν	kinematic viscosity
μ	viscosity
λ	non-dimensional parameter
ρ	density
τ_X	dimensionless local skin friction
$\overline{\tau}$	dimensionless average skin friction

Subscripts

i	designates grid points along the X-direction
j	designates grid points along the R-direction

DOI: 10.1002/fld

w conditions on the wall
∞ free stream conditions

Superscripts

n time-step level

ACKNOWLEDGEMENTS

This work was supported by BK21 Research Programme, Inha University, Republic of Korea.

REFERENCES

1. Sparrow EM, Gregg JL. Laminar-free convection heat transfer from the outer surface of a vertical circular cylinder. *Transactions of the ASME* 1956; **78**:1823–1829.
2. Minkowycz WJ, Sparrow EM. Local nonsimilar solutions for natural convection on vertical cylinder. *Journal of Heat Transfer* 1974; **96**:178–183.
3. Lee HR, Chen TS, Armaly BF. Natural convection along slender vertical cylinders with variable surface temperature. *Journal of Heat Transfer* 1988; **110**:103–108.
4. Ganesan P, Rani HP. Transient natural convection flow over vertical cylinder with variable surface temperatures. *Forschung im Ingeneieurwesen* 2000; **66**:11–16.
5. Saffman PG. On the stability of laminar flow of a dusty gas. *Journal of Fluid Mechanics* 1962; **13**:120–128.
6. Liu JTC. Flow induced by an oscillating infinite plat plate in a dusty gas. *Physics of Fluids* 1966; **9**:1716–1720.
7. Michael DH, Miller DA. Plane parallel flow of a dusty gas. *Mathematika* 1966; **13**:97–109.
8. Michael DH. The steady motion of a sphere in a dusty gas. *Journal of Fluid Mechanics* 1968; **31**(1):175–192.
9. Soundalgekar VM, Gokhale MY. Flow of a dusty gas past an impulsively started infinite vertical plate. *Regional Journal of Energy Heat and Mass Transfer* 1984; **6**:289–295.
10. Das UN, Ray SN, Soundalgekar VM. Flow of a dusty gas past an accelerated infinite horizontal plate-finite difference solution. *Indian Journal of Technology* 1992; **30**:327–329.
11. Palani G, Ganesan P. Heat transfer effects on dusty gas flow past a semi-infinite inclined plate. *Forschung im Ingeneieurwesen* 2007; **71**:223–230.
12. Carnahan B, Luther HA, Wilkes JO. *Applied Numerical Methods*. Wiley: New York, 1969.
13. Schlichting H. *Boundary Layer Theory*. McGraw-Hill: New York, 1979.
14. Carslaw HS, Jaeger JC. *Conduction of Heat in Solids*. Oxford University Press: London, 1959.

DOI: 10.1002/fld